Liquid−Solid Process for Growing Gold Nanowires on an Indium Tin Oxide Substrate as Excellent Field Emitters

Chih-Yen Chen,[†] Kai-Yuan Cheng,[†] Yen-Chang Chu,[†] Lih-Juann Chen,[†] Wei-Leun Fang,[‡] Chia-Seng Chang,[§] and Li-Jen Chou*,[†]

[†]Department of Materials Science and Engineering and [‡]Department of Power Mechanical Engineering, National Tsing Hua University, Hsinchu, 30013 Taiwan

[§]Institutes of Physics, Academia Sinica, Nankang, Taipei 115, Taiwan

Ⓢ Supporting Information

ABSTRACT: Gold nanowires are successfully grown on an ITO substrate by a liquid−solid process. An excellent field emission behavior of the nanowires, as indicated by the field enhancement factor (β) of up to 7585, indicates a significant decrease in energy barrier between the nanowires and the ITO substrate. A single Au nanowire demonstrates a strong emission current up to 800 nA at an applied voltage of 200 V. The outstanding reliability of the nanowires warrants their potential applications as effective electron field emitters and chemical and/or biological sensors in future microelectronics.
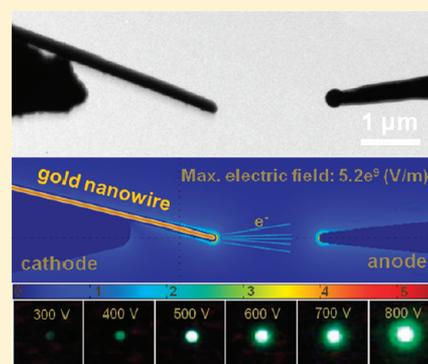
One-dimensional (1-D) nanostructures such as nanowires (NWs), nanotubes, and nanobelts have been widely used for fabrication of electronic and field emission devices.[1−4] One-dimensional noble nanowires possess excellent electrical and thermal conductivity, the very best malleability and ductility, and high chemical inertness property.[5] Au nanostructures have been widely investigated for a century due to its easy fabrication and many possible applications. Takayanagi et al. investigated the behavior of electron transport through 1-D nanoscale Au channels.[6,7] With all of these attractive merits, Au nanomaterials are most promising for applications, such as nanoelectronic interconnects,[6−8] optical transport behavior,[9] chemical sensors,[10] and biomedical or biosensing devices.[11] There are many reports about the synthesis techniques of gold nanostructures such as oxidation reduction,[12,13] electrochemical process,[14,15] or template fabrications.[16]

However, the synthesis method employing liquid−solid (L−S) mechanism has yet to be explored. In this study, we report a simple, low-temperature (∼400 °C) synthesis method to grow single-crystal Au nanowires on an indium tin oxide (ITO) substrate via the L−S growth process. These nanowires are approximately 100 nm in diameter and 10 μm in length. The field emission characteristics of Au nanowires have been studied, and the results indicate that the Au nanowires have a great potential to be used for field emission and sensor applications.

■ RESULTS AND DISCUSSION

ITO substrates are selected for the growth of Au nanowires. A 500 nm Ti thin film to be followed with a 100 nm Au film has

been deposited on the ITO by e-beam deposition at a pressure below 10⁻⁶ Torr. We have designed a unique method to grow single-crystal Au nanowires with high aspect ratio through a L−S mechanism. The L−S process takes place in two steps. It starts with the formation of liquid Au−Ti droplets first to be followed by the growth of solid Au nanowires.

Figure 1 illustrates a schematic growth model of the single-crystal Au nanowires form at low temperature on the ITO substrate. Previous investigations of the binary Au−Ti system have shown that Au−Ti solid solution may form above 400 °C.[17,18] During the nucleation step, the Au/Ti multilayer transforms and separates tiny Au−Ti nanoparticles having Au concentration close to be ∼99% form on the ITO substrate when the sample is annealed at temperature around 500 °C for 60 min. These Au-rich nanoparticles serve as the bases for the nanowires growth, as shown in Figure 1a. In the second step, extra colloidal gold nanoparticles which have been synthesized by oleylamine/oleic acid system[12,13] are poured onto the existing Au-rich nanoparticles before the substrate are quickly placed in the furnace. It is suggested that colloidal gold nanoparticles deposited on the Au-rich nanoparticles transform to form Au needle points due to a cooperative-controlled crystallization mechanism.[19] The extra colloidal gold in the organic solvent can play a role in the synthesis process, such as precursor and seed concentration and size, as well as providing an optimal temperature and surface diffusion rate for reaction.
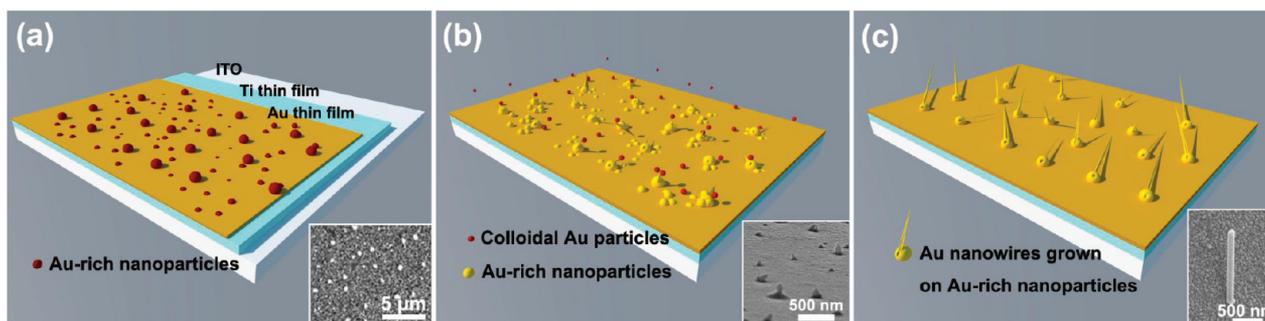
Figure 1. Schematics depict the growth model for Au nanowires on ITO substrates. The SEM insets (a−c) illustrate the corresponding growth steps (a−c).

Therefore, Au NWs are precipitated from the interface of the Au supersaturated needle points as shown in Figure 1b. In an effort to synthesize free-standing Au nanowires by self-assembly in a fluid, Au vapor would serve as an additional source for nanowires growth. Eventually, in Figure 1c, the free-standing Au nanowires are grown on the ITO surface. More scanning electron microscopy (SEM) images, optical microscopy (OM) images, and EDS analysis for growth descriptions of Au nanowires are presented in Figure S1 in the Supporting Information.

Figure 2a shows the SEM morphology of nanowires grown via L−S growth process on the ITO substrate. The nanowires are about 10−15 μm in length. Parts b−d of Figure 2 show a TEM image of an individual Au nanowire, its corresponding high-angle annular dark field (HAADF) image and energy
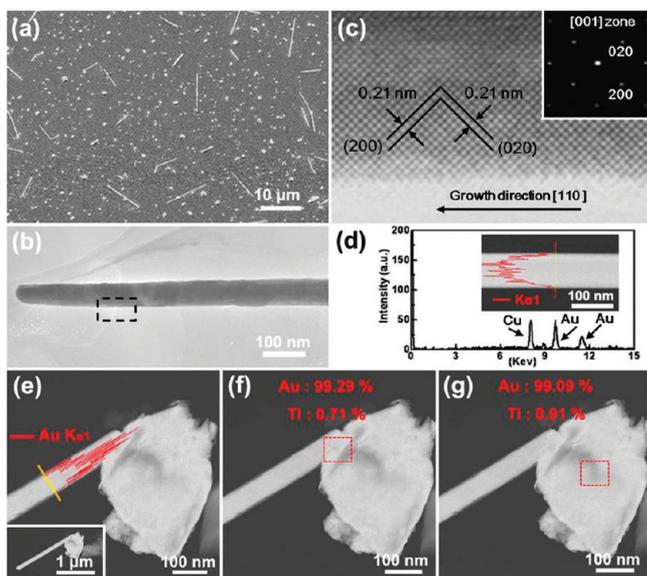
Figure 2. (a) SEM image of free-standing Au nanowires grown on ITO substrate. The average length of Au nanowires is about 10−15 μm. (b) High-magnification TEM image revealing the diameter of Au nanowire is close to 100 nm. (c) High-resolution TEM image corresponding to the Au nanowire in b. The inset displays the SAD patterns with the [001] zone of the Au nanowire. (d) HAADF TEM image and its corresponding EDS line-scan profile. (e) HAADF image and the line-scanned EDS result of an individual Au nanowire. (f) Showing the mapping composition results at the root of the Au nanowire indicating the presence of Au−Ti alloy. (g) Mapping result revealing the composition at the interface between the Au nanowire and the root.

dispersive spectrometer (EDS) spectrum, respectively. Figure 2c is the corresponding high-resolution TEM image of the Au nanowire; it shows a prefect single-crystal structure of our Au nanowire. Furthermore, the interplanar distances between (002) and (020) planes are both 0.21 nm. A selected-area diffraction (SAD) pattern with [001] zone axis matches well with the reported data of the Au NW which is a face centered cubic crystal (fcc) structure, with $a = b = c = 4.0786$ Å, and it belongs to the symmetry group of $Fm\overline{3}m$.[20] The SAD study of a representative Au NW also displays a composite pattern that originated with [110] growth orientation. Some previous reports have been shown their Au nanowires fabricated with the same direction.[21,22] On the basis of the results, we suggest that the Au nanoparticles may inhibit the growth of Au facets in multiple dimensions so that the deposition of Au atoms on Au (220) becomes a preferred orientation. Parts e−g of Figure 2 are the HAADF images of a single Au NW; each highlights a different region of the NW for detailed analysis. Figure 2e shows a line-scan result of the Au nanowire, and a uniform composition is obtained. Figure 2f shows that the concentrations of Au and Ti at the interface between the Au NW and its root region are 99.29% and 0.71%. Figure 2g indicates that the Au and Ti ratio in the root region is 99.09% vs 0.91%, respectively. The slight increase of Au in the nanowire as compared to that in the root region suggests that Au atoms are pulled from the root region of Au-rich nanoparticles for the nanowire growth via the L−S mechanism.

For the electric field emitter made with Au nanowires grown on a designed area (∼1 cm^2) of the ITO plate, Figure 3 shows the field emission characteristics of the device including Figure 3a for the current density versus applied electric field, Figure 3b for the typical Fowler−Nordheim plot, and Figure 3c for the reliability test. The distance between the anode and cathode was fixed at 100 μm. The ITO coated with phosphor was used for plate screen measurement, and the Au nanowire emitters were chosen as the cathode. The presented data (Figure 3a) are repeatedly measured over 50 times without fluctuation. The turn-on field is defined as the applied voltage needed to produce an emitting current density of 0.01 mA/cm^2. The inset indicates that the single-crystal Au nanowires on ITO substrate exhibit a turn-on field around 2.5−3 V/μm. The maximum emission current can reach up to 1.5 mA/cm^2, as the applied voltage increases over 1000 V. Even after 50 tests, Au nanowire emitters still possess more than 60% of its peak value. The Au nanowires synthesized through the L−S method are single crystal in structure. They are different from the polycrystalline nanowires grown by these processes.[12−16] Since the conductivity for single-crystal Au nanowires is better than that of

12825

dx.doi.org/10.1021/jp212583k | J. Phys. Chem. C 2012, 116, 12824−12828
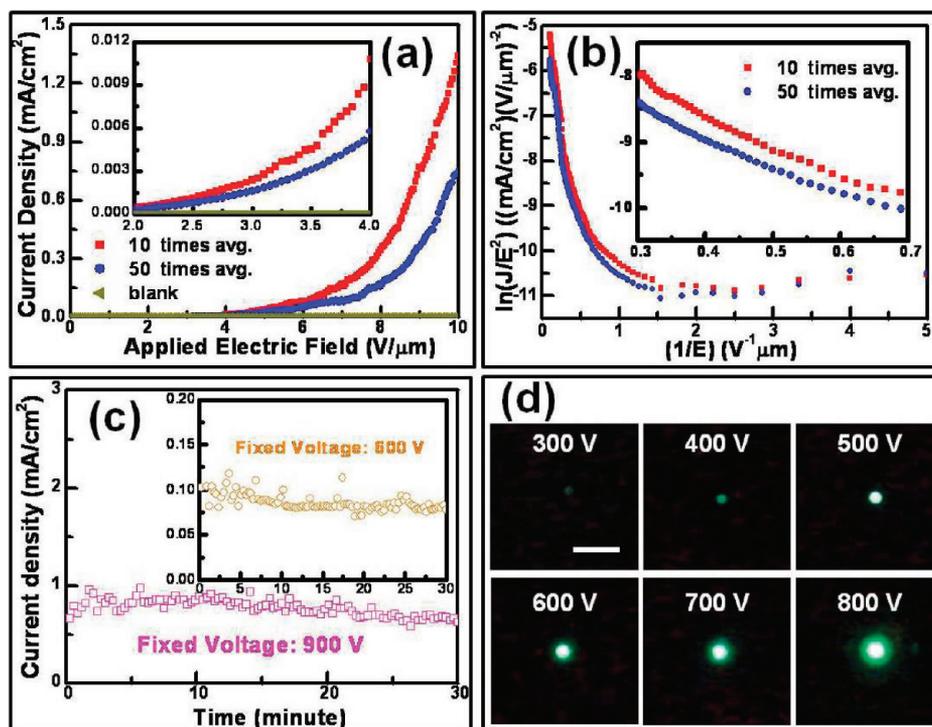
Figure 3. Field-emission current as a function of applied electric field at 100 μm between emitters and anode. Panels a and b represent the electric field emission behaviors and the corresponding $\ln(J/E^2)-(1/E)$ plots of the field emission device, respectively. The data were recorded for a series of experiments, denoted as average values of the initial 10 and the total 50 measurements. (c) Showing the reliability tests conducted at a fixed voltage of 600 and 900 V overtime. (d) Displaying the fluorescent light-emitting photographs under several different applied voltages. The scale bar denotes 1 cm.

the polycrystalline Au nanowires, higher emission current density and larger field enhancement factor (β) are achieved. Our Au nanowires have shown much better emission properties than those reported from metallic emitters such as $TaSi_2$,[23] $TiSi_2$,[24] Ti_5Si_3,[25] Ni_2Si,[26] Cr_5Si_3,[27] and CoSi nanowires.[28]

Figure 3b shows the corresponding Fowler−Nordheim plots ($\ln(J/E^2)-(1/E)$ curve) of the device after 10 and 50 tests, respectively; the current−voltage equation is given as follows:[29]

$$ J = \left(\frac{A\beta^2 E^2}{\Phi}\right)\exp\left(-\frac{B\Phi^{3/2}}{\beta E}\right) $$

where J is the current density, E is the applied field strength, and Φ is the work function. A and B are constants, corresponding to 1.56×10^{-10} A V^{-2} eV and 6.83×10^3 V eV$^{-3/2}$ μm^{-1}, respectively. The β factor, representing the quality of the field emission for the tip shape on a planar surface, can be estimated from the slope ($-B\Phi^{3/2}/\beta$) of the F−N plot. At high applied field, the β value indicates that the barrier-tunneling mechanism is responsible for the field emission. From the measurements with a work function value at 5.1 eV,[30] the calculated β value of the single-crystal Au nanowires is about 7585 in the initial 10 tests. After 50 tests, the β value is still round at 7187, which is much higher than the previous report.[14−16,23−28] This high β value should result from the better conductivity between the Au nanowires and ITO substrate, and the low screening effect of the sample. Besides, a good ohmic contact is achieved between Au nanowire and ITO substrate. To further explain the so great β values of our device, a model of high-current field emission with a simple band diagram between the Ti thin film layer and n-type ITO substrate is proposed[31,32] in Figure S2 in the Supporting

Information. Low resistance of the Au nanowire itself also provides good conductivity for the electron transport which leads to the high-current field emission and high field enhancement factor.[33] On the other hand, attributed to the lower density of the Au nanowires on the ITO substrate, from the simulation results in Figures S3 and S4 in the Supporting Information, the screening effect which will reduce the field emission characteristics such as the field enhancement factor is minimal in our device.

Since device reliability is the most important factor that decides if a device has any potential to become commercially viable. We thus put on Au nanowire emitters on a stress test. As shown in Figure 3c, the Au nanowires field emitters have been tested under a high operating voltage at 600 and 900 V for 30 min. At 900 V, the emission current reaches around 0.772 mA/cm^2 with a standard deviation of 0.084 mA/cm^2. The inset also shows the emission current and standard deviation to be 0.086 mA/cm^2 and 0.009 mA/cm^2 at 600 V, respectively. The reliability results of the Au nanowire field emitters are promising. Figure 3d shows the fluorescent light-emitting images of the emitter taken from the front cathode plate, as the device varies from 300 to 800 V.

To further investigate the field emission properties of an individual Au nanowire, Figure 4 shows the results of an Au nanowire tested in situ within a TEM. Figure 4a illustrates the in situ field emission measurement setup in an in situ ultrahigh-vacuum transmission electron microscopy (UHV-TEM). A single Au nanowire is attached on a commercial gold needle by using a conductive silver paste. The distance between the anode and Au emitter is 500 nm. The single Au nanowire exhibits a turn-on voltage of 130 V, as indicated by a blue arrow, and the maximum emission current is up to 800 nA at an applied
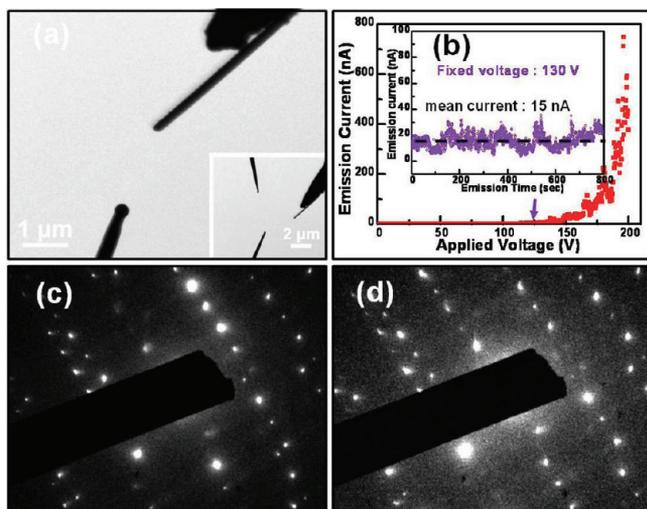
Figure 4. Field-emission current as a function of applied electric field between the individual Au nanowire and anode. (a) High-magnification TEM image and its inset describe a measurement setup in an in situ UHV-TEM. (b) Inset representing the field emission behavior of an individual Au nanowire and its corresponding durability test at 130 V overtime. (c and d) SAD patterns at the initial and final experimental conditions. No significant changes are observed in c and d.

voltage of 200 V in Figure 4b. Although the value is less than the best reported values of the single-walled carbon nanotube (SWCNT) and the single pure ZrO/W nanowire,[34,35] it is much better than other emitters such as ZnO nanowire,[33] multiwalled carbon nanotube (MWCNT), and TaSi$_2$ nanowires.[36,37] The inset of Figure 4b shows, in a reliability test of an Au nanowire, the emission current is stable around 15 nA at 130 V for a 15 min continuous operation.

Meanwhile, we also simulate the outstanding experimental emission results of the individual Au nanowire by using the finite element method. The calculated results with the COMSOL 3.3 software are shown in the Supporting Information. The simulated results show that if the applied voltage reaches at 200 V, the highest electric field at the corner area can reach up to 5.2×10^9 V/m. Figure S5c presents the equipotential distributions while the nanodevice is turned on. Other simulation data are also given in Figure S5 in Supporting Information. Parts c and d of Figure 4 show the SAD pattern images before and after the emission tests, respectively. They provide the direct evidence that the microstructure of this Au nanowire undergoing a 15 min harsh emission test at an applied voltage of 130 V does not change at all.

CONCLUSIONS

In summary, free-standing and single-crystal Au nanowires have been successfully fabricated at low temperature by a liquid–solid (L–S) growth process. The morphology of Au nanowires is needlelike with lengths up to 15 μm and the average diameter of Au nanowire about 100 nm. The electric field emitters made by Au nanowires on the large-scale devices and a nano field emitter made by an individual Au nanowire have been investigated. The single-crystal Au nanowires exhibit outstanding properties at the lowest turn-on field of 3–3.5 V/μm and the maximum current density of 1.5 mA/cm^2. A reproducible value of the field enhancement factor is close to 7585 due to higher conductivity between Au nanowires and

ITO substrate and the low screening effect. The reliability tests indicate that the emission current of the Au nanowire field emitter is very stable under a high operating voltage of 600 and 900 V for 30 min. An Au nanowire emission study also demonstrates a strong emission current up to 800 nA at an applied voltage of 200 V. A nearly constant emission current is obtained at an applied voltage of 130 V for 15 min. TEM investigation also confirmed the unchanged microstructures of the Au nanowire before and after the emission test. The above outstanding results warrant possible applications for Au nanowires as the electron field emitters and chemical and/or biological sensors in future microelectronics.

EXPERIMENTAL METHODS

A horizontal three-zone tube furnace system, including a mechanical pump, a gas flow system, and a quartz tube alumina tube combo, is used to synthesize the nanowires. The vacuum level is higher than 1×10^{-2} Torr, and the maximum annealing temperature is up to 1500 °C. Indium tin oxide substrates are selected for the growth of Au nanowires. Prior to the growth of nanowires, ITO substrates are consecutively cleaned by ultrasonication with acetone and deionized water. The Ti and Au thin films are deposited separately on the ITO by e-beam deposition under the pressure of 1.0×10^{-6} Torr. The extra colloidal gold nanoparticles have been synthesized by a chemical reflux method. A 150 mg amount of chloroauric acid (HAuCl$_4$) is mixed with 800 μL of oleylamine and 400 μL of oleic acid in 100 mL of toluene, and refluxed at 120 °C for several hours. The nanowires have been characterized using a field emission transmission electron microscope (FE-TEM, JEM-3000F) provided with an EDS equipment used to obtain the chemical compositions of the microstructures. The Z-contrast images are obtained by a HAADF detector to detect the electrons scattered at high angles. The TEM sample is prepared by ultrasonic treatment, where nanowires are removed and dispersed in isopropyl alcohol (IPA) and several drops of the dispersion are placed to conventional carbon-coated copper grids. The field emission current is measured below 1×10^{-6} Torr at room temperature. The distance between the anode and the emitting surface is fixed at 100 μm. In addition, the nanoscale field emission current of an individual Au nanowire has been carried out in an in situ ultrahigh-vacuum TEM (in situ UHV-TEM, JEM-2000 V), which is combined with a scanning tunneling microscope (STM) with a nanooperation system. The system included mechanical motions in three dimensions, and the fine adjustments are performed with a piezo-tube scanner. The lowest emission current is recorded on the level of picoampere (pA).

ASSOCIATED CONTENT

S **Supporting Information**

Text discussing extra characterization of Au NP or NW, figures showing SEM images of Au NPs and OM pictures of Au NPs and NWs, a band diagram between the Ti thin film and ITO, four simulations results of the equipotential lines, simulation results revealing the corresponding electric field, electric field changes in simulation results and emitting current density, and simulations results of an individual Au nanowire, and a table listing simulatin parameters. This material is available free of charge via the Internet at http://pubs.acs.org.

AUTHOR INFORMATION

Corresponding Author
*E-mail: ljchou@mx.nthu.edu.tw.

Notes
The authors declare no competing financial interest.

REFERENCES

(1) Yang, C.; Zhong, Z. H.; Lieber, C. M. *Science* **2005**, *310*, 1304−1307.

(2) Xia, Y. N.; Yang, P. D.; Sun, Y. G.; Wu, Y. Y.; Mayers, B.; Gates, B.; Yin, Y. D.; Kim, F.; Yan, Y. Q. *Adv. Mater.* **2003**, *15* (5), 353−389.

(3) Pan, Z. W.; Dai, Z. R.; Wang, Z. L. *Science* **2001**, *291*, 1947−1949.

(4) Chen, C. Y.; Lin, Y. K.; Hsu, C. W.; Wang, C. Y.; Chueh, Y. L.; Chen, L. J.; Lo, S. C.; Chou, L. J. *Nano Lett.* **2012**, *12*, 2254−2259.

(5) Chen, J. Y.; Wiley, B. J.; Xia, Y. N. *Langmuir* **2007**, *23*, 4120−4129.

(6) Ohnishi, H.; Kondo, Y.; Takayanagi, K. *Nature* **1998**, *395* (6704), 780−783.

(7) Kondo, Y.; Takayanagi, K. *Science* **2000**, *289*, 606−608.

(8) Corti, C. W.; Holliday, R. J.; Thompson, D. T. *Gold Bull.* **2002**, *35* (4), 111−117.

(9) Chen, P. H.; Hsieh, C. H.; Chen, S. Y.; Wu, C. H.; Wu, Y. J.; Chou, L. J.; Chen, L. J. *Nano Lett.* **2010**, *10*, 3267−3271.

(10) Lu, Y.; Yang, M.; Qu, F.; Shen, G.; Yu, R. *Bioelectrochemistry* **2007**, *71*, 211−216.

(11) Djalali, R.; Chen, Y.; Matsui, H. *J. Am. Chem. Soc.* **2002**, *124*, 13660−13661.

(12) Halder, A.; Ravishankar, N. *Adv. Mater.* **2007**, *19* (14), 1854−+.

(13) Huo, Z. Y.; Tsung, C. K.; Huang, W. Y.; Zhang, X. F.; Yang, P. D. *Nano Lett.* **2008**, *8*, 2041−2044.

(14) Dangwal, A.; Pandey, C. S.; Muller, G.; Karim, S.; Cornelius, T. W.; Trautmann, C. *Appl. Phys. Lett.* **2008**, *92*, 6.

(15) Navitski, A.; Muller, G.; Sakharuk, V.; Cornelius, T. W.; Trautmann, C.; Karim, S. *Eur. Phys. J.: Appl. Phys.* **2009**, *48*, 3.

(16) Zhang, G. M.; Emmanuel, R.; Liu, H. W.; Liu, W. M.; Hou, S. M.; Kui, Y. Z.; Xue, Z. Q. *Chin. Phys. Lett.* **2002**, *19* (7), 1016−1018.

(17) Okamoto, H.; Massalski, T. B. *Phase Diagrams of Binary Gold Alloys*; American Society for Metals International: Materials Park, OH, USA, 1987.

(18) Tepper, T.; Shechtman, D.; vanHeerden, D.; Josell, D. *Mater. Lett.* **1997**, *33* (3−4), 181−184.

(19) Pong, B. K.; Elim, H. I.; Chong, J. X.; Ji, W.; Trout, B. L.; Lee, J. Y. *J. Phys. Chem. C* **2007**, *111*, 6281−6287.

(20) Swanson, H. E.; Fuyat, R. K.; Ugrinic, G. M. *National Bureau of Standards Circular* **1954**.

(21) Ozturk, B.; Flanders, B. N.; Grischkowsky, D. R.; Mishima, T. D. *Nanotechnology* **2007**, *18*, 175707−1757014.

(22) Huang, T. K.; Chen, Y. C.; Ko, H. C.; Huang, H. W.; Wang, C. H.; Lin, H. K.; Chen, F. R.; Kai, J. J.; Lee, C. Y.; Chiu, H. T. *Langmuir* **2008**, *24*, 5647−5649.

(23) Chueh, Y. L.; Ko, M. T.; Chou, L. J.; Chen, L. J.; Wu, C. S.; Chen, C. D. *Nano Lett.* **2006**, *6*, 1637−1644.

(24) Chang, C. M.; Chang, Y. C.; Chung, Y. A.; Lee, C. Y.; Chen, L. J. *J. Phys. Chem. C* **2009**, *113*, 17720−17723.

(25) Lin, H. K.; Tzeng, Y. F.; Wang, C. H.; Tai, N. H.; Lin, I. N.; Lee, C. Y.; Chiu, H. T. *Chem. Mater.* **2008**, *20*, 2429−2431.

(26) Liu, Z. H.; Zhang, H.; Wang, L.; Yang, D. R. *Nanotechnology* **2008**, *19*, 37.

(27) Chang, M. T.; Chen, C. Y.; Chou, L. J.; Chen, L. J. *ACS Nano* **2009**, *3*, 3776−3780.

(28) Tsai, C. I.; Yeh, P. H.; Wang, C. Y.; Wu, H. W.; Chen, U. S.; Lu, M. Y.; Wu, W. W.; Chen, L. J.; Wang, Z. L. *Cryst. Growth Des.* **2009**, *9* (10), 4514−4518.

(29) Fowler, R. H.; Nordheim, L. Electron emission in intense electric fields. *Proc. R. Soc. London, Ser. A* **1928**, *119* (781), 173−181.

(30) Michaelson, H. B. *J. Appl. Phys.* **1977**, *48* (11), 4729−4733.

(31) Pradhan, D.; Kumar, M.; Ando, Y.; Leung, K. T. *Nanotechnology* **2008**, *19*, 3.

(32) Huang, K.; Pan, Q. T.; Yang, F.; Ni, S. B.; He, D. Y. *Mater. Res. Bull.* **2008**, *43* (4), 919−925.

(33) She, J. C.; Xiao, Z. M.; Yang, Y. H.; Deng, S. Z.; Chen, J.; Yang, G. W.; Xu, N. S. *ACS Nano* **2008**, *2*, 2015−2022.

(34) Xu, Z.; Bai, X. D.; Wang, E. G.; Wang, Z. L. *Appl. Phys. Lett.* **2005**, *87*, 16.

(35) Fursey, G. N.; Baskin, L. M.; Glazanov, D. V.; Yevgen'ev, A. O.; Kotcheryzhenkov, A. V.; Polezhaev, S. A. *J. Vac. Sci. Technol. B* **1998**, *16* (1), 232−237.

(36) Ribaya, B. P.; Leung, J.; Brown, P.; Rahman, M.; Nguyen, C. V. *Nanotechnology* **2008**, *19*, 18.

(37) Kim, J. J.; Shindo, D.; Murakami, Y.; Xia, W.; Chou, L. J.; Chueh, Y. L. *Nano Lett.* **2007**, *7*, 2243−2247.